Materials Advances

ROYAL SOCIETY OF CHEMISTRY

REVIEW

View Article Online
View Journal | View Issue

Cite this: *Mater. Adv.*, 2020, **1**, 2155

Visible-light-driven organic transformations integrated with H_2 production on semiconductors

Jian-Hong Tang and Yujie Sun *

Received 18th May 2020,
Accepted 27th July 2020

DOI: 10.1039/d0ma00327a

rsc.li/materials-advances

Due to its clean and sustainable nature, solar energy has been widely recognized as a green energy source in driving a variety of reactions, ranging from small molecule activation and organic transformation to biomass valorization. Within this context, organic reactions coupled with H_2 evolution *via* semiconductor-based photocatalytic systems under visible light irradiation have gained increasing attention in recent years, which utilize both excited electrons and holes generated on semiconductors and produce two types of value-added products, organics and H_2, simultaneously. Based on the nature of the organic reactions, in this review article we classify semiconductor-based photocatalytic organic transformations and H_2 evolution into three categories: (i) photocatalytic organic oxidation reactions coupled with H_2 production, including oxidative upgrading of alcohols and biomass-derived intermediate compounds; (ii) photocatalytic oxidative coupling reactions integrated with H_2 generation, such as C–C, C–N, and S–S coupling reactions; and (iii) photo-reforming reactions together with H_2 formation using organic plastics, pollutants, and biomass as the substrates. Representative heterogeneous photocatalytic systems will be highlighted. Specific emphasis will be placed on their synthesis, characterization, and photocatalytic mechanism, as well as the organic reaction scope and practical application.

1. Introduction

The exploration of sustainable and renewable energy sources has received increasing attention in order to reduce our dependence on finite and environmentally unfriendly fossil reserves.[1–3] Solar energy, as one of the most green and abundant renewable energy sources, represents a promising candidate, which can be directly converted to chemical energy *via* photocatalysis.[4,5] Among various photocatalytic systems, semiconductor-based photocatalytic H_2 production integrated with organic transformations not only directly produces H_2 as the cleanest energy carrier and chemical fuel but also has potential to generate value-added organic products.[6–9] In this process, photo-excited electrons of irradiated semiconductors reduce protons to yield H_2, while the resulting holes simultaneously drive oxidative organic transformations (Scheme 1).

Given the fact that the major component of the solar spectrum falls in the range of 400–700 nm, it is critical to develop visible light-absorbing photocatalytic systems in order to effectively capture solar irradiation and hence achieve a high solar energy conversion efficiency.[10–12] In this regard, homogeneous photocatalysts consisting of transition metal complexes or organic dye molecules whose absorption spectra cover the visible region have been widely investigated for photocatalytic H_2 evolution and organic transformations. Nevertheless, the challenging separation of these molecular photocatalysts and/or sensitizers from reaction media, together with their questionable long-term stability, represents apparent drawbacks of their practical application on a large scale.[11] Comparatively, heterogeneous photocatalysts can be phase-separated from most products and also tend to exhibit better durability. Hence, visible light-responsive heterogeneous photocatalysts are highly desirable for H_2 production coupled with organic oxidations. Among a wide array of heterogeneous photocatalysts, semiconductors ranging from transition metal oxides and sulphides to metal-free carbon nitrides have emerged as the most representative visible light-active solid-state photocatalysts.[13–15]

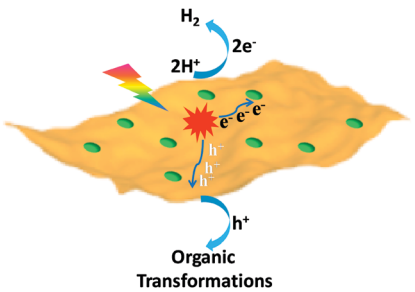

Scheme 1 Schematic representation of the dual function of a semiconductor-based photocatalyst for integrated H_2 evolution and organic transformations.

Department of Chemistry, University of Cincinnati, Cincinnati, OH 45221, USA. E-mail: yujie.sun@uc.edu

In the last several years, the research field of semiconductor-based photocatalysis for selective organic transformations integrated with the production of clean and carbon-free H_2 has made significant advancements.[6,7,9,16] A diverse array of organic reactions coupled with H_2 production have been realized such as the oxidation of alcohols and biomass-derived intermediate compounds, C–C, C–N, and S–S coupling reactions, degradation of plastics and pollutants, and biomass photo-reforming reactions. In this review, we focus on visible light-driven photocatalysis consisting of semiconductors and aim to summarize the recent progress in this infant research field. Specifically, we will discuss the synthesis, characterization, and photocatalytic mechanism, and performance of each photocatalytic system in specific organic reactions. The current advances and critical issues in this field will also be highlighted.

2. Photocatalytic organic oxidation coupled with H_2 production

2.1 Integration of H_2 production with the oxidation of alkyl or aryl alcohols

Visible-light-driven photocatalytic oxidation of alcohols to their corresponding carbonyl compounds with concurrent H_2 generation is a promising strategy for solar energy conversion and storage in value-added chemicals and fuels. Recently, a large amount of semiconductor-based photocatalysts have been developed for oxidizing alkyl or aryl alcohols to aldehydes and/or ketones coupled with H_2 production by simultaneously utilizing photogenerated electrons and holes (Scheme 2).

In 2013, Higashimoto *et al.* reported a Pd-deposited CdS–TiO_2 photocatalyst for the selective oxidation of benzyl alcohol to benzaldehyde accompanied by H_2 evolution under visible light irradiation.[17] The synergistic effects of CdS, TiO_2, and Pd species enhanced the photocatalytic activities with high selectivity (>99%), wherein CdS–TiO_2 works as the photo-responsive center, while the Pd species act as the co-catalyst. Moreover, this photocatalytic system was able to drive the oxidation of a large scope of benzyl alcohol derivatives with substituents from electron-donating (*p*-OH, *m*-OCH_3 and *p*-CH_3) to electron-withdrawing groups (*p*-Cl). Recently, a noble-metal-free Ni/CdS photocatalyst (Ni nanocrystal-modified CdS nanoparticles) for transforming alcohols to corresponding aldehydes or ketones and H_2 was reported by Xu and co-workers (Fig. 1a).[18] *In situ* photodeposition was employed to decorate the CdS surface with Ni nanocrystals to prepare the target photocatalyst. The high-resolution transmission electron microscopy (HRTEM) image of Ni/CdS indicated that metallic Ni nanoparticles with lattice distances of (111) and (200) were successfully deposited on the CdS surface (Fig. 1b). As shown in Fig. 1c, a series of control samples were investigated to probe the impact

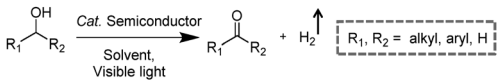

Scheme 2 Representative photocatalytic oxidation of alcohols.

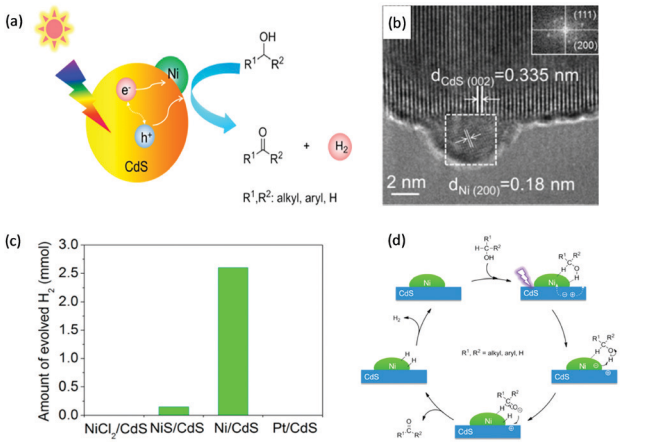

Fig. 1 (a) Schematic representation of visible light-driven alcohol oxidation coupled with H_2 evolution on a Ni/CdS photocatalyst. (b) HRTEM image of Ni/CdS (the inset image is the Fourier transform of the marked area). (c) Produced H_2 amount during the photocatalytic oxidation of 2-propanol using different photocatalysts. (d) Proposed mechanism for the photocatalytic alcohol oxidation coupled with H_2 evolution. Reprinted from ref. 18 with permission from American Chemical Society, copyright 2016.

of various co-catalysts on CdS, which revealed the important role played by the synergistic effect between Ni and CdS. Accordingly, the authors proposed a photocatalytic mechanism of Ni/CdS for efficient alcohol oxidation coupled with H_2 production. As shown in Fig. 1d, firstly, a photo-excited electron on CdS reacts with a proton that is abstracted from the alcohol substrate to afford Ni–H and an alkoxide anion. The alkoxide anion is then oxidized by the photo-excited hole to generate another Ni–H and produce the corresponding aldehyde or ketone. Finally, two resulting Ni–H form one H_2.

Besides CdS-based photocatalysts,[17–21] several other categories of semiconductor-based photocatalysts have also been investigated for the selective oxidation of alcohols, such as $Zn_3In_2S_6$,[22] g-C_3N_4,[23] and $SrTiO_3$.[24] For instance, $Zn_3In_2S_6$ photocatalysts were prepared *via* a facile solvothermal method for the selective transformation of aromatic alcohols to aldehydes and H_2 under visible light irradiation.[22] Recently, Wu and co-workers unveiled a CdSe quantum dot photocatalyst capped with 3-mercaptopropionic acid (denoted as MPA-CdSe QD) for efficient photo-oxidation of alcohols to carbonyl compounds. Upon visible light irradiation, a wide array of alcohols can be selectively oxidized to the corresponding aldehydes/ketones using Ni^{2+} ions as a H_2 evolution cocatalyst, and 3-mercaptopropionic acid and water as relay reagents.[25]

2.2 Integration of H_2 production with oxidative valorization of biomass-derived intermediate compounds

Following the growing interest in exploring green carbon resources as an alternative to fossil reserves, biomass valorization has attracted increasing attention. Consequently, a large amount of effort has been devoted to developing photocatalytic systems for the solar-driven upgrading of biomass-derived intermediate compounds.[26–31] Compared to the use of traditional hole scavengers in photocatalytic H_2 production, which inevitably

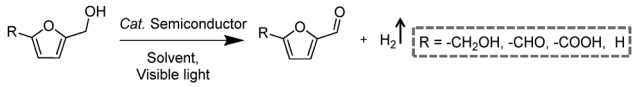

Scheme 3 Representative photocatalytic oxidation of biomass-derived intermediate compounds.

leads to the increase of cost and production of waste, renewable biomass and biomass-based intermediates are not only able to consume the photo-excited holes but also produce value-added chemicals in addition to H_2. To date, considerable advances have been achieved in this emerging research field (Scheme 3).

Among many biomass-derived intermediate compounds, furanics are considered as platform chemicals in that they can be converted to a variety of valuable products. Sun *et al.* reported the selective upgrading of furfural alcohol and 5-hydroxymethylfurfural (HMF) to their corresponding aldehydes and acids with concomitant production of H_2 utilizing ultrathin Ni/CdS nanosheets as the co-photocatalysts (Fig. 2).[30] In neutral water, both furfural alcohol and HMF were transformed to aldehydes with distinct reaction rates as rationalized by theoretical calculations. It was found that HMF exhibited a much slower conversion rate, probably due to the slightly stronger binding affinity of the aldehyde group in HMF relative to its alcohol group as supported by the theoretical computation results. In comparison, quantitative carboxylate products could be obtained from both furfural alcohol and HMF if the photocatalysis was conducted under alkaline conditions. Therefore, it was feasible to selectively produce either furanic-derived aldehydes or acids *via* fine tuning the reaction conditions.

By using a low-temperature wet chemistry method, Xu *et al.* prepared a photocatalyst of $Ti_3C_2T_x$/CdS, which was also able to drive the photo-oxidation of furfural alcohol to furfural together with the production of H_2.[27] $Ti_3C_2T_x$ was used to capture the photo-generated electrons in CdS, accelerating the separation and transport of photo-excited charge carriers and enhancing the photocatalytic performance. Kailasam and co-workers reported the selective oxidation of HMF to 2,5-diformylfuran (DFF) with >99% selectivity by using porous carbon nitride as a photocatalyst and Pt as a co-catalyst.[28] Porous carbon nitride absorbs visible light to generate holes and electrons. Pt facilitates charge separation and improves the production of H_2. The photocatalytic reaction achieved a DFF yield of 13.8% and a H_2 production rate of 12 mmol h^{-1} m^{-2} after 6 h irradiation with visible light. Furthermore, a 7.2% yield of DFF production and a 6.2 mmol h^{-1} m^{-2} rate of H_2 evolution were obtained under natural sunlight for 6 h.

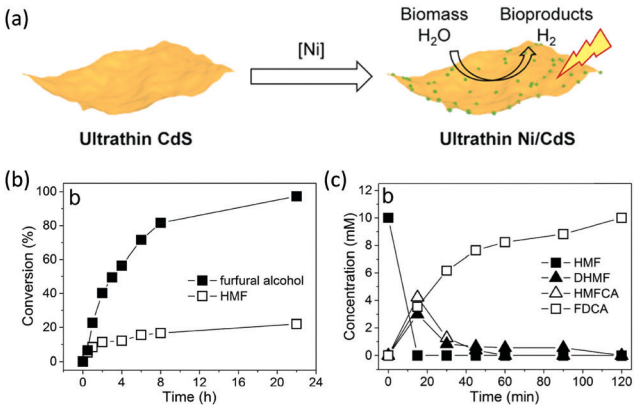

Fig. 2 (a) Synthetic route of ultrathin Ni/CdS nanosheets for integrated H_2 production and biomass valorization. (b) Concentration change over time for the photocatalytic oxidation of furfural alcohol and HMF under neutral conditions. (c) Concentration change over time for the photocatalysis of HMF under alkaline conditions. Reprinted from ref. 30 with permission from American Chemical Society, copyright 2017.

3. Photocatalytic oxidative coupling reactions integrated with H_2 generation

3.1 Integration of H_2 production with C–C coupling reactions

In addition to the unimolecular oxidation reactions for the consumption of photo-generated holes, bimolecular oxidative coupling reactions can also be achieved on semiconductors under visible light irradiation with simultaneous H_2 production (Scheme 4).[32–35] For instance, Xie and co-workers reported a CdS nanorod photocatalyst decorated with MoS_2 nanofoams for the direct conversion of methanol to ethylene glycol (EG) with 90% selectivity and high efficiency together with H_2 production upon visible light irradiation.[33] CdS enables the facile generation of $^{\bullet}CH_2OH$ for subsequent C–C coupling and the MoS_2 nanofoam co-catalyst improves the evolution of H_2 and the overall photocatalytic activity. A concerted proton–electron transfer mechanism was proposed wherein a hydroxymethyl radical ($^{\bullet}CH_2OH$) intermediate was formed after the selective activation of the C–H bond in methanol. The weak adsorption of $^{\bullet}CH_2OH$ and CH_3OH on the catalyst surface facilitates the C–C coupling reaction and decreases the possibility of O–H bond activation of CH_3OH. Very recently, as shown in Fig. 3a, the same group developed an environmentally friendly CoP/$Zn_2In_2S_5$ catalyst *via* a simple low-temperature hydrothermal and ultrasonic method for transforming methanol to EG under visible-light irradiation without using the toxic Cd metal element.[32] CoP in the hybrid CoP/$Zn_2In_2S_5$ photocatalyst facilitates charge separation and promotes its photocatalytic performance for the formation of both EG and H_2. $Zn_2In_2S_5$ was demonstrated to selectively activate the α-C–H bond in alcohols without affecting the O–H group. Besides, this catalytic system was also demonstrated to be effective for the coupling of ethanol to 2,3-butanediol arising from the formation of the $^{\bullet}CH(OH)CH_3$ radical. Mechanistic studies indicated that the redox potential of $Zn_mIn_2S_{m+3}$ was substantially more positive than that of EG/CH_3OH (Fig. 3b), which provided sufficient

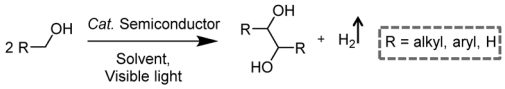

Scheme 4 Representative photocatalytic C–C coupling reaction.

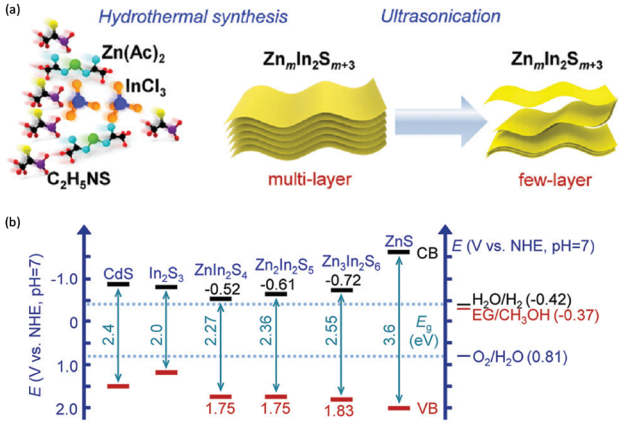

Fig. 3 (a) Schematic illustration of the low-temperature hydrothermal and ultrasonic process used to synthesize $Zn_mIn_2S_{m+3}$. (b) Energy levels of several related redox couples and band-edge positions of selected semiconductors. Reprinted from ref. 32 with permission from Royal Society of Chemistry, copyright 2020.

redox power for the oxidative coupling of methanol to EG and ethanol to 2,3-butanediol with the co-production of H_2.

Besides alcohols, C–H bonds in furanics could also be activated for C–C coupling reactions on semiconductor-based photocatalysts. Recently, Wang *et al.* reported a Ru-doped $ZnIn_2S_4$ photocatalyst, which was prepared following a one-pot hydrothermal method, in order to achieve the dehydrogenative C–C coupling of lignocellulose-derived methylfurans to diesel fuel precursors and H_2 under visible light irradiation.[34] Benefiting from the Ru dopants to improve the light harvesting and charge separation efficiency, this Ru–$ZnIn_2S_4$ photocatalyst showed decent performance with a diesel fuel precursor production rate of 1.04 g $g_{catalyst}^{-1}$ h^{-1} and high selectivity (>96%), as well as a H_2 production rate of 6.0 mmol $g_{catalyst}^{-1}$ h^{-1}. Subsequent hydrodeoxygenation treatment of the obtained coupling products of furanics would result in the desired diesel fuels containing straight- and branched-chain alkanes. By modulating the Zn/In ratio in the ZnIn sulfides, the same group also demonstrated controllable production of deoxybenzoin or benzoin from benzyl alcohol integrated with H_2 evolution under visible light irradiation.[35] It's worth noting that they successfully synthesized deoxybenzoin derivatives on a gram scale by using this photocatalytic system.

3.2 Integration of H_2 production with C–N coupling reactions

Photocatalytic C–N coupling of amines integrated with H_2 production on semiconductors has emerged as a mild and green method for the efficient synthesis of imines, which have important applications in the research fields of pharmaceuticals and agricultural chemistry (Scheme 5).[36–38] For example,

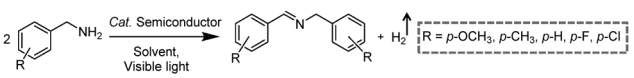

Scheme 5 Representative photocatalytic C–N coupling reaction.

Ni/CdS was reported to be able to photocatalyze the C–N coupling of amines to produce imines under visible light irradiation, while H_2 was produced in the meantime.[37] Specifically, the synthesized Ni/CdS nanoparticles showed superior benzylamine conversion (close to 100%) and excellent imine selectivity (97%). The maximum H_2 production rate was 21.4 mmol g^{-1} h^{-1} with an apparent quantum yield of 11.2%. Compared to the use of common sacrificial reagents such as TEOA or Na_2S/Na_2SO_3, the H_2 production rate increased two orders of magnitude when integrated with C–N coupling of amines to imines. Moreover, the obtained photocatalysts can be recycled several times without visible photocatalytic activity loss, indicating their robust stability and recyclability. A plausible mechanism was proposed that photo-excited electrons on CdS rapidly migrated to Ni nanoparticles to reduce protons to H_2, while photo-excited holes generated carbon cationic species to afford the target imine product. This photocatalyst also exhibited great tolerance of a wide substrate scope with various substituents on aryl amines with outstanding photocatalytic performance.

By rational design, Zhang *et al.* developed nickel-decorated ultrathin CdS nanosheet (Ni/CdS) photocatalysts with significantly enhanced photocatalytic performance (Fig. 4a) for the C–N coupling of amines. As shown in Fig. 4b, the high resolution transmission electron microscopy image of Ni/CdS showed the uniform deposition of Ni clusters on the two-dimensional ultrathin CdS nanosheets. A remarkable apparent quantum yield of 44% together with high efficiency and excellent stability was realized under visible light irradiation (Fig. 4c and d). The kinetic study of H_{ads} desorption to form molecular H_2 indicated that the Ni clusters on CdS were the active sites to promote the recombination of H_{ads}. The photo-generated holes on the surface of CdS oxidize amines to aldimine intermediates and generate protons. Another amine molecule reacts with the aldimine intermediate to form the imine and NH_3. A series of

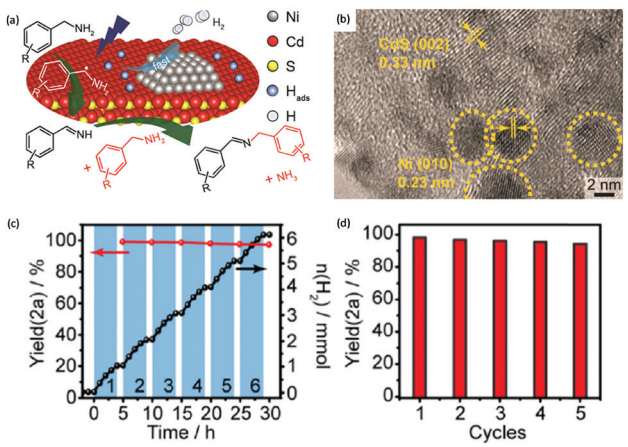

Fig. 4 (a) Schematic representation of nickel-decorated ultrathin CdS nanosheets as photocatalysts for the C–N coupling of amines to imines. (b) HRTEM of the Ni/CdS photocatalyst. (c) Photocatalytic performance of Ni/CdS for the production of imines and H_2 during photolysis. (d) Stability test of Ni/CdS for five consecutive photolysis experiments. Reprinted from ref. 36 with permission from American Chemical Society, copyright 2020.

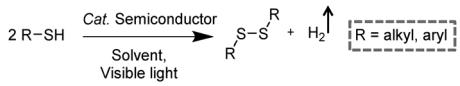

Scheme 6 Representative photocatalytic S–S coupling reaction.

primary and secondary amines with different functional groups were feasible to be coupled on Ni/CdS, suggesting a great universality of the ultrathin Ni/CdS nanosheets for the C–N coupling of many amines to yield value-added chemicals.[36]

3.3 Integration of H_2 production with S–S coupling reactions

Disulfides, as a category of important chemicals that contain S–S bonds, have attracted extensive research interest in synthetic chemistry, pharmaceuticals, and materials science (Scheme 6).[39] Traditional synthetic approaches of disulfides usually rely on the oxidative coupling of thiols, which are hindered by limitations like over-oxidized byproducts, complicated purification processes, and the requirement for expensive reagents.[40,41] Recently, photocatalytic S–S coupling for the selective and efficient conversion of thiols into disulfides and H_2 has been reported under visible-light irradiation without the requirement for any sacrificial reagent or oxidant.[42,43] For instance, Li *et al.* reported PtS/$ZnIn_2S_4$ nanocomposites for the photocatalytic S–S coupling of thiols to produce disulfides and H_2.[42] The photocatalyst was prepared by photo-reduction of $[PtCl_6]^{2-}$ on $ZnIn_2S_4$ and the resulting PtS/$ZnIn_2S_4$ displayed high stability and recyclability. The optimum photocatalytic performance of 0.5 wt% PtS/$ZnIn_2S_4$ showed a complete transformation of thiols to disulfides and H_2 in 6 h under visible light irradiation without over-oxidized products. It was demonstrated that PtS acted as an efficient hydrogen evolution co-catalyst to enhance the photocatalytic behavior of PtS/$ZnIn_2S_4$ nanocomposites, which could be applied in transforming various thiols into their corresponding disulfides ranging from benzyl mercaptanes with different substituents to furfuryl mercaptan and thiophenols.

4. Photo-reforming reaction together with H_2 generation

4.1 Integration of H_2 production with the photo-reforming of organic plastics and pollutants

Photo-reforming of organic plastics and pollutants to less-hazardous products with the concurrent production of H_2 not only reduces the global environmental crisis but also produces a green energy carrier and clean chemical feedstock, H_2 (Scheme 7). As such, Reisner *et al.* reported inexpensive CdS/CdO_x quantum dots as photocatalysts to convert plastic waste into H_2 and organic products such as formate, acetate, and pyruvate *via* visible light-driven photo-reforming (Fig. 5a and b).[44] The bulk

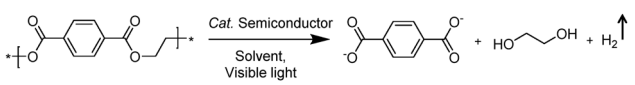

Scheme 7 Representative photo-reforming of polyethylene terephthalate (PET).

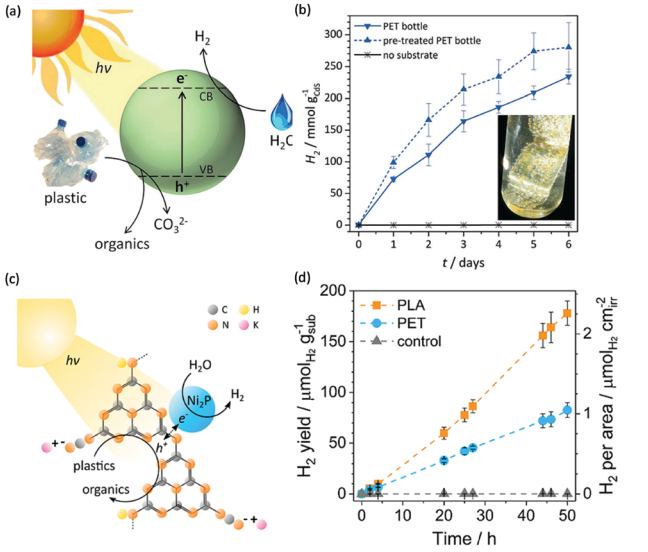

Fig. 5 (a) Schematic photo-reforming of plastic to organics *via* CdS/CdO_x quantum dots with the co-production of H_2 in alkaline aqueous media. (b) Produced H_2 amount of the photo-reforming of PET bottles under simulated solar irradiation over several days. Reprinted from ref. 44 with the permission of Royal Society of Chemistry, copyright 2018. (c) Schematic diagram of the polymer photo-reforming process using a CN_x|Ni_2P photocatalyst. (d) Produced H_2 amount of the photo-reforming of PET and PLA. Reprinted from ref. 45 with permission of American Chemical Society, copyright 2019.

band gap (2.4 eV) and band positions (CB: −0.5 V *vs.* NHE, VB: +1.9 V *vs.* NHE) of CdS enable its visible light absorption and photo-reforming reactions without a co-catalyst. It's worth noting that this reaction system enables photo-reforming a variety of plastics in a straightforward manner, including polyethylene terephthalate (PET), polylactic acid (PLA), and polyurethane. More attractively, even real plastic samples were tested for photo-reforming using the CdS/CdO_x photocatalysts and a H_2 generation activity of up to 4.13 ± 0.40 $mmol_{H_2}$ g_{CdS}^{-1} h^{-1} with an external quantum yield of 2.17 ± 0.38% and conversion of 5.15 ± 0.72% was achieved under visible light irradiation for 6 days. Considering the toxicity of Cd in CdS/CdO_x, the same group further developed a Cd-free carbon nitride/nickel phosphide (CN_x|Ni_2P) alternative for photo-reforming of plastic waste (Fig. 5c).[45] As shown in Fig. 5d, photo-irradiation of PET and PLA in the presence of CN_x|Ni_2P for 50 h produced 82.5 ± 7.3 and 178 ± 12 μmol_{H_2} g_{sub}^{-1} H_2 with turnover numbers of 7.8 ± 0.7 and 16.8 ± 1.1 mol_{H_2} mol_{Ni}^{-1}, respectively. The CN_x|Ni_2P photo-reforming system can also transform real-world polymer samples to H_2, such as polyester microfibers and oil-contaminated PET. It was proposed that the strong binding ability between the Ni_2P cocatalyst and CN_x facilitated photo-induced charge separation and enhanced the photocatalytic performance.

Other less toxic semiconductor-based photocatalytic systems have also been explored. For instance, a $ZnIn_2S_4$@SiO_2@TiO_2 (ZIS@SiO_2@TiO_2) ternary heterostructure photocatalyst was prepared following facile sol–gel and solvothermal methods and the resulting ZIS@SiO_2@TiO_2 exhibited good activity for the degradation of photocatalytic organic pollutants coupled

with H_2 production. The optimized 150%-ZIS@SiO_2@TiO_2 catalyst could produce H_2 at an excellent rate of 618.3 μmol g^{-1} h^{-1} and 99.7% efficiency was achieved for the degradation of methylene blue under simulated sunlight. Compared to the binary ZIS@SiO_2 and ZIS@TiO_2 counterparts, the ternary ZIS@SiO_2@TiO_2 possessed better photocatalytic performance under identical conditions. It was rationalized that the heterojunction in ZIS@SiO_2@TiO_2 enhanced the separation and transportation efficiency of electron–hole pairs, which was beneficial for outstanding photocatalytic activity.[46]

4.2 Integration of H_2 production with biomass photo-reforming

H_2 production arising from biomass-based photo-reforming is regarded as a direct and sustainable route to utilize renewable carbon resources to produce green fuels as alternatives to fossil fuels (Scheme 8). In 2017, Wakerley *et al.* reported a CdS/CdO_x photocatalyst for the photo-reforming of cellulose, hemicellulose, and lignin to H_2 under alkaline conditions.[47] Moreover, unprocessed lignocelluloses, such as wood and paper, were also able to be reformed under solar irradiation together with H_2 production. The photocatalytic mechanism involved the formation of an oxide/hydroxide *in situ* on CdS/CdO_x under alkaline conditions to improve the photo-reforming performance. To pursue an inexpensive, non-toxic and visible-light absorbing photocatalyst, polymeric carbon nitride (CN_x) combined with various proton reduction co-catalysts such as heterogeneous Pt or MoS_2 and a molecular Ni bis(diphosphine) catalyst (NiP) was also developed by the same group for the photo-reforming of biomass to yield H_2 (Fig. 6a). They demonstrated that various purified lignocellulosic components and even raw biomass substrates were able to be photo-reformed to generate H_2 using activated $^{NCN}CN_x$ and NiP as a H_2 evolution co-catalyst (Fig. 6b). It was found that ultra-sonication activated cyanamide-functionalized carbon nitride exhibited an enhanced photo-reforming performance under aqueous conditions with tolerance of a wide pH window (pH = 2–15).[48]

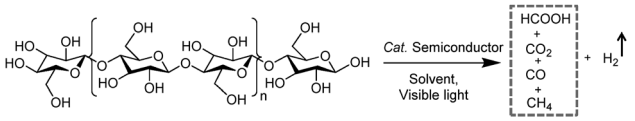

Scheme 8 Representative photo-reforming of cellulose into H_2.

Very recently, Wang *et al.* developed an ethyl alcohol grafted carbon nitride photocatalyst through an *in situ* C–N coupling method which showed enhanced visible light absorption, increased charge density, and prolonged lifetime of excited charges relative to pristine carbon nitride. In the presence of Pt co-catalysts, the ethyl alcohol grafted carbon nitride exhibited superior visible light-driven activity for the photo-reforming of several monosaccharides to produce H_2.[49]

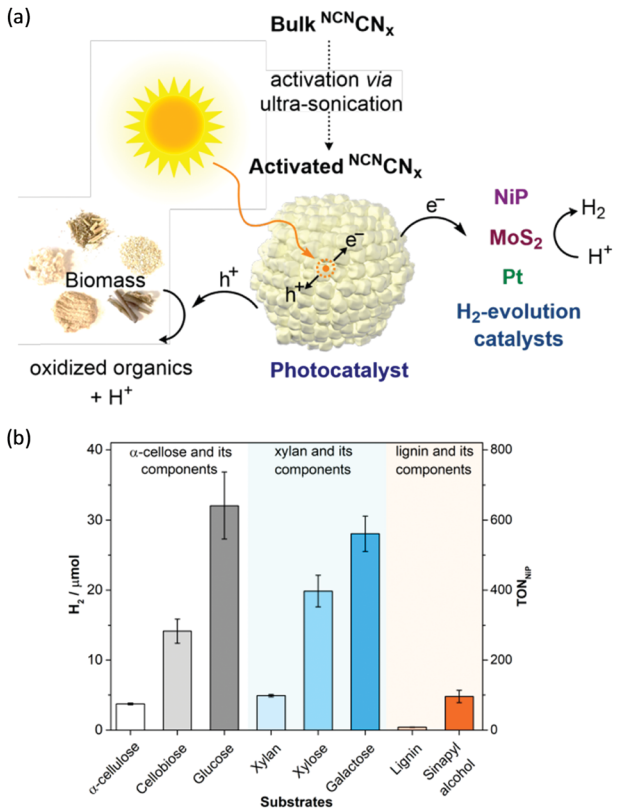

Fig. 6 (a) Schematic photo-reforming of lignocellulose using $^{NCN}CN_x$ and proton reduction co-catalysts. (b) Photocatalytic H_2 production from purified lignocellulose components catalyzed by activated $^{NCN}CN_x$ and NiP under AM1.5G light irradiation for one day at 25 °C. Reprinted from ref. 48 with permission of American Chemical Society, copyright 2018.

5. Conclusion and outlook

Visible light-driven organic transformation integrated with H_2 production on semiconductors represents an efficient approach for solar to chemical conversion. According to the nature of the organic reactions, we have presented three representative categories of organic transformations coupled with H_2 evolution: (i) photocatalytic organic oxidation, (ii) photocatalytic oxidative coupling, and (iii) photo-reforming reactions. It is apparent that a number of semiconductor-based photocatalytic systems have been developed to drive a wide range of organic reactions with the aim of producing value-added chemicals and H_2 simultaneously under visible light irradiation. Even though in all the discussed photocatalytic reactions there is one basic principle that all of the organic substrates act as hole scavengers, the rational design of semiconductor-based photocatalysts indeed plays a vital role in controlling the efficiency, selectivity, durability, and scope of the overall reactions. For instance, for integrated H_2 evolution with photocatalytic alcohol oxidation, Ni/CdS NPs exhibit a much higher rate of H_2 production relative to NiS/CdS NPs, while $NiCl_2$/CdS NPs are unable to catalyze this reaction.

Despite the rapid advancement in this emerging research field, there are several issues that should be addressed before practical application on a large scale. Firstly, given the requirement for long-term operation and environmental friendliness,

it is of critical importance to develop non-toxic semiconductor-based photocatalysts with high efficiency, selectivity, and durability. As implied in the aforementioned examples, Cd-based chalcogenides have been widely utilized; however, the toxicity of Cd and the potential for self-oxidation due to the chalcogenide anions would restrict their practical employment. In contrast, metal-free carbon-based photocatalysts tend to exhibit better stability, in addition to their more benign and inexpensive nature. However, in terms of photocatalytic activity, carbon-based photocatalysts are currently inferior to the metal-based counterparts. Future research efforts should be devoted to designing and synthesizing novel semiconductors with better visible light absorption, long-lived excited pairs, and sufficient redox power. Secondly, investigation of reaction mechanisms should be conducted at the molecular and even atomic level by using *in situ* techniques and theoretical calculations. Unveiling the catalytic mechanism is anticipated to elucidate the structure–performance relationship of photocatalysts and provide guidance for the above rational design of high-performance photocatalysts. Thirdly, in addition to typical batch-type reactors for photocatalysis in research laboratories, it is more appealing to assemble larger-scale photo-reactors, preferably flow reactors, to demonstrate the real promise of any developed photocatalytic systems for practical applications under solar irradiation.

Conflicts of interest

There are no conflicts to declare.

Acknowledgements

Y. S. acknowledges the financial support of the Herman Frasch Foundation (820-HF17), National Science Foundation (CHE1914546), and the University of Cincinnati.

References

1 L. A. Weinstein, J. Loomis, B. Bhatia, D. M. Bierman, E. N. Wang and G. Chen, *Chem. Rev.*, 2015, **115**, 12797–12838.
2 J. Gong, C. Li and M. R. Wasielewski, *Chem. Soc. Rev.*, 2019, **48**, 1862–1864.
3 E. Gies, *Nature*, 2017, **551**, S145–S147.
4 X. Yang and D. Wang, *ACS Appl. Energy Mater.*, 2018, **1**, 6657–6693.
5 Y. Tachibana, L. Vayssieres and J. R. Durrant, *Nat. Photonics*, 2012, **6**, 511.
6 S. Kampouri and K. C. Stylianou, *ACS Catal.*, 2019, **9**, 4247–4270.
7 F. Wang, Q. Li and D. Xu, *Adv. Energy Mater.*, 2017, **7**, 1700529.
8 X. Liu, X. Duan, W. Wei, S. Wang and B.-J. Ni, *Green Chem.*, 2019, **21**, 4266–4289.
9 B. Xia, Y. Zhang, B. Shi, J. Ran, K. Davey and S. Z. Qiao, *Small Methods*, 2020, 2000063.
10 J. M. Narayanam and C. R. Stephenson, *Chem. Soc. Rev.*, 2011, **40**, 102–113.
11 C. K. Prier, D. A. Rankic and D. W. MacMillan, *Chem. Rev.*, 2013, **113**, 5322–5363.
12 L. Marzo, S. K. Pagire, O. Reiser and B. König, *Angew. Chem., Int. Ed.*, 2018, **57**, 10034–10072.
13 H. Hao and X. Lang, *ChemCatChem*, 2019, **11**, 1378–1393.
14 H. Kisch, *Angew. Chem., Int. Ed.*, 2013, **52**, 812–847.
15 I. Ghosh, J. Khamrai, A. Savateev, N. Shlapakov, M. Antonietti and B. König, *Science*, 2019, **365**, 360–366.
16 B. You, G. Han and Y. Sun, *Chem. Commun.*, 2018, **54**, 5943–5955.
17 S. Higashimoto, Y. Tanaka, R. Ishikawa, S. Hasegawa, M. Azuma, H. Ohue and Y. Sakata, *Catal. Sci. Technol.*, 2013, **3**, 400–403.
18 Z. Chai, T.-T. Zeng, Q. Li, L.-Q. Lu, W.-J. Xiao and D. Xu, *J. Am. Chem. Soc.*, 2016, **138**, 10128–10131.
19 D. Jiang, X. Chen, Z. Zhang, L. Zhang, Y. Wang, Z. Sun, R. M. Irfan and P. Du, *J. Catal.*, 2018, **357**, 147–153.
20 Y. Xu, L.-Z. Zeng, Z.-C. Fu, C. Li, Z. Yang, Y. Chen and W.-F. Fu, *Catal. Sci. Technol.*, 2018, **8**, 2540–2545.
21 Y. Chao, J. Lai, Y. Yang, P. Zhou, Y. Zhang, Z. Mu, S. Li, J. Zheng, Z. Zhu and Y. Tan, *Catal. Sci. Technol.*, 2018, **8**, 3372–3378.
22 X. Ye, Y. Chen, Y. Wu, X. Zhang, X. Wang and S. Chen, *Appl. Catal., B*, 2019, **242**, 302–311.
23 F. Li, Y. Wang, J. Du, Y. Zhu, C. Xu and L. Sun, *Appl. Catal., B*, 2018, **225**, 258–263.
24 Y. Hu, G. Zhao, Q. Pan, H. Wang, Z. Shen, B. Peng, G. W. Busser, X. Wang and M. Muhler, *ChemCatChem*, 2019, **11**, 5139–5144.
25 L.-M. Zhao, Q.-Y. Meng, X.-B. Fan, C. Ye, X.-B. Li, B. Chen, V. Ramamurthy, C.-H. Tung and L.-Z. Wu, *Angew. Chem., Int. Ed.*, 2017, **56**, 3020–3024.
26 H.-F. Ye, R. Shi, X. Yang, W.-F. Fu and Y. Chen, *Appl. Catal., B*, 2018, **233**, 70–79.
27 Y.-H. Li, F. Zhang, Y. Chen, J.-Y. Li and Y.-J. Xu, *Green Chem.*, 2020, **22**, 163–169.
28 V. R. Battula, A. Jaryal and K. Kailasam, *J. Mater. Chem. A*, 2019, **7**, 5643–5649.
29 Y. Wang, X. Kong, M. Jiang, F. Zhang and X. Lei, *Inorg. Chem. Front.*, 2020, **7**, 437–446.
30 G. Han, Y.-H. Jin, R. A. Burgess, N. E. Dickenson, X.-M. Cao and Y. Sun, *J. Am. Chem. Soc.*, 2017, **139**, 15584–15587.
31 H. G. Cha and K.-S. Choi, *Nat. Chem.*, 2015, **7**, 328.
32 H. Zhang, S. Xie, J. Hu, X. Wu, Q. Zhang, J. Cheng and Y. Wang, *Chem. Commun.*, 2020, **56**, 1776–1779.
33 S. Xie, Z. Shen, J. Deng, P. Guo, Q. Zhang, H. Zhang, C. Ma, Z. Jiang, J. Cheng, D. Deng and Y. Wang, *Nat. Commun.*, 2018, **9**, 1–7.
34 N. Luo, T. Montini, J. Zhang, P. Fornasiero, E. Fonda, T. Hou, W. Nie, J. Lu, J. Liu, M. Heggen, L. Lin, C. Ma, M. Wang, F. Fan, S. Jin and F. Wang, *Nat. Energy*, 2019, **4**, 575–584.
35 N. Luo, T. Hou, S. Liu, B. Zeng, J. Lu, J. Zhang, H. Li and F. Wang, *ACS Catal.*, 2020, **10**, 762–769.
36 Y. Huang, C. Liu, M. Li, H. Li, Y. Li, R. Su and B. Zhang, *ACS Catal.*, 2020, **10**, 3904–3910.
37 W. Yu, D. Zhang, X. Guo, C. Song and Z. Zhao, *Catal. Sci. Technol.*, 2018, **8**, 5148–5154.

38 Y. Xiao, G. Tian, W. Li, Y. Xie, B. Jiang, C. Tian, D. Zhao and H. Fu, *J. Am. Chem. Soc.*, 2019, **141**, 2508–2515.
39 A. M. Almeida, R. Li and S. H. Gellman, *J. Am. Chem. Soc.*, 2012, **134**, 75–78.
40 A. R. Hajipour, S. E. Mallakpour and H. Adibi, *J. Org. Chem.*, 2002, **67**, 8666–8668.
41 J. B. Arterburn, M. C. Perry, S. L. Nelson, B. R. Dible and M. S. Holguin, *J. Am. Chem. Soc.*, 1997, **119**, 9309–9310.
42 L. Xu, X. Deng and Z. Li, *Appl. Catal., B*, 2018, **234**, 50–55.
43 X. B. Li, Z. J. Li, Y. J. Gao, Q. Y. Meng, S. Yu, R. G. Weiss, C. H. Tung and L. Z. Wu, *Angew. Chem., Int. Ed.*, 2014, **53**, 2085–2089.
44 T. Uekert, M. F. Kuehnel, D. W. Wakerley and E. Reisner, *Energy Environ. Sci.*, 2018, **11**, 2853–2857.
45 T. Uekert, H. Kasap and E. Reisner, *J. Am. Chem. Soc.*, 2019, **141**, 15201–15210.
46 L. Wang, H. Zhou, H. Zhang, Y. Song, H. Zhang and X. Qian, *Inorg. Chem.*, 2020, **59**, 2278–2287.
47 D. W. Wakerley, M. F. Kuehnel, K. L. Orchard, K. H. Ly, T. E. Rosser and E. Reisner, *Nat. Energy*, 2017, **2**, 17021.
48 H. Kasap, D. S. Achilleos, A. Huang and E. Reisner, *J. Am. Chem. Soc.*, 2018, **140**, 11604–11607.
49 Q. Liu, L. Wei, Q. Xi, Y. Lei and F. Wang, *Chem. Eng. J.*, 2020, **383**, 123792.

